Scaling of the localization length in armchair-edge graphene nanoribbons

D. Gunlycke and C. T. White
Naval Research Laboratory, Washington, DC 20375, USA

(Received 3 November 2009; revised manuscript received 22 December 2009; published 24 February 2010)

A two-band model that includes edge interactions is derived for hydrogen-terminated, armchair-edge graphene nanoribbons. This model is then used to obtain analytical expressions for the localization length of these ribbons in the presence of environmental and topological edge disorder. Within the single-channel regime, it is found that the maximum localization length of a ribbon with uncorrelated edge disorder is proportional to the square of its width. Also shown is the dependence of the localization length on quasiparticle energy and band gap. The analytical expressions have been verified by numerical transport calculations that take all π channels into account.

DOI: 10.1103/PhysRevB.81.075434 PACS number(s): 73.22.Dj, 73.61.Wp, 73.63.Bd

I. INTRODUCTION

Because of their relationship to carbon nanotubes,[1,2] graphene ribbons could potentially offer room-temperature ballistic transport at the micrometer scale.[3] Unlike carbon nanotubes, however, graphene ribbons have edges that are vulnerable to disorder[4–15] that could limit the localization length,[4,5] and hence, the length over which ballistic transport could occur. There are two types of edge disorder: environmental and topological. Environmental edge disorder is recognized by a disordered potential at the ribbon edges, which for instance, is present in ribbons with two or more edge terminations that randomly occupy the edge sites. Topological edge disorder, on the other hand, is disorder among the carbon interaction paths at the edges. An example of the latter type of disorder is edge roughness. Both types of disorder can be present in experiments, and therefore, their tendency to localize quasiparticle (electron or hole) wave functions within ribbons needs to be further understood.

In a typical conducting wire with residual disorder, the mean-free path is independent of the size of the wire. If the wire is planar, the number of edge atoms is independent of the width W of the wire, while the total number of atoms is proportional to W; hence, edge disorder only acts on a small ratio of atoms that is inversely proportional to W. It is therefore reasonable to expect that the mean-free path due to edge disorder scales with W. Near the Fermi level in armchair-edge graphene nanoribbons, however, this expectation would be misleading. Herein, analytical expressions for the localization length, which is related to the mean-free path, are presented for the single-channel regime near the Fermi level. The derivations are based on a two-band model that reproduces the band dispersions near the Fermi level of conduction and valence bands obtained through first-principles methods.[16,17] Environmental and topological edge disorder have been modeled by Anderson disorder[18] and by an edge roughness algorithm,[5] respectively. The expressions for both types of disorder reveal some interesting scaling behavior: (i) the localization length ξ is the longest in the linear dispersion regime, where it scales as $\xi \propto W^2$. (ii) In the regime near the conduction- and valence-band edges, where the dispersion is parabolic, the localization length scales as $\xi \propto W^3$. This scaling does not owe its presence to the parabolic dispersion but rather the inverse width dependence of the effective mass. Therefore, this scaling is not expected to be present in wires characterized by a constant effective mass, which are often assumed (see, e.g., Ref. 19). (iii) If the energy is scaled with the band gap, the localization length scales as $\xi \propto W^2$, regardless of weather the system is in the linear or parabolic regime. (iv) The maximum localization length is largely independent of the graphene π-hopping parameter γ, for topological edge disorder, while $\xi_{\max} \propto \gamma^2$ for environmental edge disorder. (v) The slope of the localization length scales as $\partial\xi/\partial E \propto W^3$. That the maximum localization length in the linear dispersion regime scales as $\xi \propto W^2$ can partly explain why ballistic transport, so far, has been difficult to observe in experiments using narrow graphene ribbons. Also, the slope of the localization length suggests that wider ribbons should offer a sharper transition between high (on) and low (off) conductance.

In the next section, the two-band model is derived. This model is then applied in Sec. III, in which different types of disorder are defined, and estimates of the localization length for ribbons subjected to these types of disorder, are presented. The derived analytical expressions, in this section, are verified by numerical multichannel transport calculations. The results from Sec. III are discussed in Sec. IV and finally some conclusions are drawn in Sec. V.

II. TWO-BAND MODEL

To reproduce first-principles band structures near the Fermi level, an orthonormal tight-binding model of hydrogen-terminated, armchair-edge graphene nanoribbons must include edge distortions[16] and third-nearest-neighbor interactions,[20] in addition to nearest-neighbor interactions. While the band structures of this model can be obtained numerically, they can generally not be obtained in an exact analytic form. Fortunately, third-nearest-neighbor interactions and edge distortions can be treated as perturbations to a nearest-neighbor Hamiltonian.[17]

The nearest-neighbor model of armchair-edge graphene ribbons is based on the nearest-neighbor model of graphene;[21] both models assume a basis set consisting of orthonormal π orbitals. The primitive cell of graphene ribbons, however, contains many more atoms than the primitive

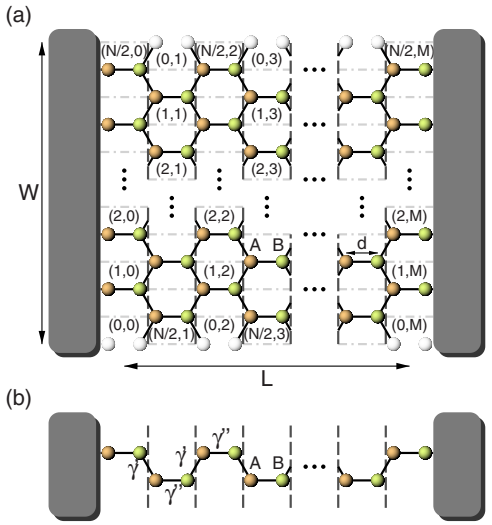

FIG. 1. (Color online) Schematic illustrations of a hydrogen-terminated, armchair-edge graphene nanoribbon with width W and length L. (a) The ribbon shown in real space. Dashed lines separate helical motifs. Dash-dotted lines divide each motif into cells (j,j') that each contains two atoms, A and B, separated by the bond length d. The cell index j' counts the motifs from left to right. j counts the cells within motif j', starting with $j=0$ for the cell that contains white hydrogen sites. (b) The ribbon representation in the two-band model described in the text, where γ' and γ'' are effective hopping parameters.

cell of graphene. Consider for notational convenience and without loss of generality, a ribbon with an arbitrary even number N of carbon atoms in the zigzag chains that extend across the strip. Helical symmetry can then be applied, which is advantageous to translational symmetry because the minimal helical motif contains, in this case, only half as many atoms as the primitive cell, thus halving the number of atoms that need to be treated explicitly. Helical symmetry allows the ribbon to be constructed by performing a π rotation about the ribbon axis for every $3d/2$ translation of the motif along the same axis, where $d\approx 0.142$ nm is the carbon-carbon bond length. These π rotations can be seen in Fig. 1(a), where the hydrogen atoms are located on one edge in one motif and on the opposite edge in neighboring motifs.

Using the site notation from Fig. 1(a), the nearest-neighbor Hamiltonian becomes

$$\hat{H}_1 = \gamma_1 \sum_{n=1}^{N/2} \sum_{m=1}^{M} [c_{n,m}^{B\dagger} c_{n,m}^{A} + c_{N/2-n+1,m-1}^{B\dagger} c_{n,m}^{A} + c_{N/2-n,m-1}^{B\dagger} c_{n,m}^{A}] + \text{H.c.}, \tag{1}$$

where $\gamma_1 \approx -3.2$ eV,[20] and $c_{j,j'}^{\tau}$ ($c_{j,j'}^{\tau\dagger}$) is an annihilation (creation) operator. The boundary condition along the ribbon axis is periodic, i.e., $c_{j,j'+M}^{\tau\dagger}|\Omega\rangle = c_{j,j'}^{\tau\dagger}|\Omega\rangle$ for all j, j', and τ, where $|\Omega\rangle$ is the vacuum state. Because the difference between the onsite energies of hydrogen and carbon is much larger than $|\gamma|$, any π-electron population on the hydrogen sites can be neglected, and consequently, the wave function must have nodes on these sites.[22] Additionally, to keep graphene solutions preserved in an infinite array of parallel ribbons, the wave function must be odd in the transverse direction at the hydrogen sites.[20] These conditions are satisfied by the transverse boundary conditions

$$\begin{cases} c_{0,j'}^{\tau\dagger}|\Omega\rangle = 0, \\ c_{N/2+1,j'}^{\tau\dagger}|\Omega\rangle = -c_{N/2,j'}^{\tau\dagger}|\Omega\rangle, \end{cases} \tag{2}$$

for all j' and τ. These boundary conditions are automatically fulfilled by the transformation[4,23,24]

$$c_{n,m}^{\tau} = \frac{2}{\sqrt{N+1}} \sum_{p=1}^{N/2} \sin\frac{2np\pi}{N+1} \tilde{c}_{p,m}^{\tau}, \tag{3}$$

which transforms the Hamiltonian in Eq. (1) to one that represents $N/2$ independent one-dimensional chains:

$$\hat{H}_1 = \sum_p \sum_m [\zeta_p \varepsilon_p \tilde{c}_{p,m-1}^{B\dagger} \tilde{c}_{p,m}^{A} + \gamma_1 \tilde{c}_{p,m}^{B\dagger} \tilde{c}_{p,m}^{A}] + \text{H.c.}, \tag{4}$$

where $\zeta_p \equiv (-1)^{p-1}$ and $\varepsilon_p \equiv 2\gamma_1 \cos[p\pi/(N+1)]$. Each chain p generates one pair of conduction and valence bands. The bands of interest herein are the two bands closest to the Fermi level, and they both come from the chain $p=p^*$, where $p^* \equiv [N+2-mod(N-1,3)]/3$. For narrow-gap armchair-edge nanoribbons, $p^*=(N+1)/3$, and for this p^*, $\zeta_{p^*}\varepsilon_{p^*}=\gamma_1$ and all chain couplings coincide. The absence of a band gap in this chain is inconsistent with the band gaps predicted by first-principles methods,[16,17,20,25] thus requiring that semiempirical models go beyond the standard nearest-neighbor model to be able to make qualitative predictions based on the band structure near the Fermi level.

The failure to predict band gaps in narrow-gap armchair-edge nanoribbons is overcome by including third-nearest-neighbor interactions and edge distortions in the model.[17] The third-nearest-neighbor Hamiltonian for one ribbon in an array of identical, parallel ribbons is

$$\hat{H}_3 = \gamma_3 \sum_{n=1}^{N/2} \sum_{m=1}^{M} [c_{n,m-1}^{B\dagger} c_{n,m+1}^{A} + c_{n+1,m}^{B\dagger} c_{n,m}^{A} + c_{n-1,m}^{B\dagger} c_{n,m}^{A}] + \text{H.c.}, \tag{5}$$

where $\gamma_3 \approx -0.3$ eV.[20] The description of isolated ribbons which have edges, requires an additional Hamiltonian which subtracts third-nearest-neighbor interactions, $-\gamma_3(c_{N/2+1,j'}^{B\dagger} c_{N/2,j'}^{A} + \text{H.c.})$, between neighboring ribbons in the parallel ribbon array.[17,20] This Hamiltonian, which only describes edge interactions, should also reflect edge distortions in the ribbons.[16] Using the boundary conditions in Eq. (2) to rewrite the third-nearest-neighbor interactions at the edges, e.g., $-\gamma_3 c_{N/2+1,j'}^{B\dagger} c_{N/2,j'}^{A} = \gamma_3 c_{N/2,j'}^{B\dagger} c_{N/2,j'}^{A}$, the edge Hamiltonian becomes

$$\hat{H}_{\text{edge}} = \sum_{m=1}^{M} [(\gamma_3 + \Delta\gamma_1) c_{N/2,m}^{B\dagger} c_{N/2,m}^{A}] + \text{H.c.}, \tag{6}$$

where $\Delta\gamma_1 \approx -0.2$ eV is an edge distortion parameter.[17] It is generally impossible to solve the eigenvalue problem that is associated with the combined Hamiltonian $\hat{H}_1 + \hat{H}_3 + \hat{H}_{\text{edge}}$. Further analytical progress can, however, be made when the

Hamiltonians, $\hat{H}_3$ and $\hat{H}_{\text{edge}}$, are treated as perturbations to the Hamiltonian $\hat{H}_1$. After transforming the combined Hamiltonian using Eq. (3), it is projected, to first order, onto $p=p^*$ to give a two-band model described by the Hamiltonian

$$\hat{H}_0 = \sum_m [\gamma' \tilde{c}_{m-1}^{B\dagger} \tilde{c}_m^A + \gamma'' \tilde{c}_m^{B\dagger} \tilde{c}_m^A] + \text{H.c.}, \tag{7}$$

where the parameters $\gamma' \approx \gamma - [1 - mod(N-1,3)]\pi\gamma/\sqrt{3}(N+1)$ and $\gamma'' \approx \gamma + 3(\gamma_3 + \Delta\gamma_1)/(N+1)$ with $\gamma \equiv \gamma_1 - 2\gamma_3 \approx -2.6$ eV. This Hamiltonian is analogous to that describing the alternating linear chain shown in Fig. 1(b). The application of the discrete Fourier transform

$$\tilde{c}_m^\tau = \frac{1}{\sqrt{M}} \sum_\kappa e^{-i\kappa m} \bar{c}_\kappa^\tau, \tag{8}$$

simplifies Eq. (7) to

$$\hat{H}_0 = \sum_\kappa [\gamma' e^{-i\kappa} + \gamma''] \bar{c}_\kappa^{B\dagger} \bar{c}_\kappa^A + \text{H.c.}, \tag{9}$$

where the helical phase κ is related to the translational wave vector k through $\kappa = 3kd/2$. From Eq. (9), it is straightforward to obtain the bands of the two-band model. Their energy dispersions are

$$\varepsilon(\kappa) = \pm \sqrt{\gamma'^2 + \gamma''^2 + 2\gamma'\gamma'' \cos\kappa}, \tag{10}$$

resulting in a band gap, $E_g = 2|\gamma' - \gamma''|$, that agrees with first-principles calculations.[17] Also needed for the localization length calculations, below, are the axial group velocity, $v \equiv d\varepsilon/\hbar dk = 3d d\varepsilon/2\hbar d\kappa$, and total density of states, $\rho = M/\pi |d\varepsilon/d\kappa| = 3Md/2\pi\hbar|v|$. To an excellent approximation near the Fermi level, the velocity of a forward-moving quasiparticle with energy E, is

$$v(E) \approx \frac{3d}{2\hbar} \left| \frac{\gamma}{E} \right| \sqrt{E^2 - \frac{E_g^2}{4}}. \tag{11}$$

Using the same approximation as in Eq. (11), the density of states becomes

$$\rho(E) \approx \frac{M}{\pi} \left| \frac{E}{\gamma} \right| \left(E^2 - \frac{E_g^2}{4} \right)^{-1/2}. \tag{12}$$

III. LOCALIZATION LENGTH

Now recall that an intrinsic property of disordered materials is the localization length.[18] If a one-dimensional disordered wire is long enough, the conductivity scales as $G(L) \propto \exp(-L/\xi)$, where ξ is one half the amplitude localization length. For weak disorder, in a single-channel regime, it has been proven that ξ equals the mean-free path of the system,[26] where the latter quantity could be derived from the Fermi golden rule, yielding

$$\xi^{-1}(E) = \frac{\pi\rho}{\hbar v} \langle |\langle -\kappa|\hat{V}|\kappa\rangle|^2 \rangle_{\text{avg}}, \tag{13}$$

where $|\kappa\rangle = (\bar{c}_\kappa^{A\dagger} \pm e^{i\theta(\kappa)} \bar{c}_\kappa^{B\dagger})|\Omega\rangle/\sqrt{2}$ is the forward-moving eigenstate of the two-band model at energy E, $\hat{V}$ is the disorder potential, and $\langle \ldots \rangle_{\text{avg}}$ denotes an ensemble average over the disorder.

Consider a nanoribbon with random uncorrelated short-range disorder. The disorder could be modeled through the application of a stochastic potential that produces random fluctuations of the onsite energies at the ribbon sites,[18] giving

$$\hat{V} = \sum_{n=1}^{N/2} \sum_{m=1}^{M} [\delta\varepsilon_{n,m}^A c_{n,m}^{A\dagger} c_{n,m}^A + \delta\varepsilon_{n,m}^B c_{n,m}^{B\dagger} c_{n,m}^B]. \tag{14}$$

The onsite energies $\delta\varepsilon_{j,j'}^\tau$ are selected from an Anderson distribution of width ΔW. The back-scattering matrix element for this potential is

$$\langle -\kappa|\hat{V}|\kappa\rangle = \frac{2}{M(N+1)} \sum_{n,m} (\delta\varepsilon_{n,m}^A + e^{2i\theta(\kappa)} \delta\varepsilon_{n,m}^B) \times \sin^2 \frac{2np^*\pi}{N+1} e^{-2i\kappa m}. \tag{15}$$

For uncorrelated onsite energies, $\langle \delta\varepsilon_{j,j'}^\tau \delta\varepsilon_{j'',j'''}^{\tau'} \rangle_{\text{avg}} = \delta_{j,j''}\delta_{j',j'''}\delta_{\tau,\tau'}\sigma_\varepsilon^2$ for all j, j', j'', j''', τ, and τ', where $\sigma_\varepsilon^2 = (\Delta W)^2/12$ is the variance of the Anderson distribution. Using these relations, together with Eqs. (11)–(13) and (15), finally leads to an expression for the localization length within the single-channel regime,

$$\xi(E) \approx \frac{2W}{\sqrt{3}} \frac{\gamma^2}{\sigma_\varepsilon^2} \left(1 - \frac{E_g^2}{4E^2} \right), \tag{16}$$

where $W = (N+1)\sqrt{3}d/2$ is the width of the strip. As expected,[4,9] this expression is inversely proportional to the variance. The upper limit for this expression—were there no band gap—is also in agreement with a previous prediction.[4] Equation (16) contains an explicit width dependence, and an implicit width dependence through the band gap E_g. Letting $E \propto E_g$ eliminates the latter width dependence, and the focus can be brought to the former explicit width dependence, which in this case is proportional to W [cf. Fig. 2(a)].

Arguably the most serious kind of disorder in graphene ribbons is edge disorder.[4,5] Edge disorder could be grouped into two classes: environmental and topological. Environmental edge disorder is defined by disorder that could be modeled through a fluctuating edge potential, whereas topological edge disorder is disorder that affects the interaction paths at the edges. The environmental edge disorder is herein modeled by the potential

$$\hat{V} = \sum_{m=1}^{M} [\delta\varepsilon_m^A c_{N/2,m}^{A\dagger} c_{N/2,m}^A + \delta\varepsilon_m^B c_{N/2,m}^{B\dagger} c_{N/2,m}^B], \tag{17}$$

where the onsite energies $\delta\varepsilon_j^\tau$ are again selected from an Anderson distribution of width ΔW. The back-scattering matrix element for the environmental edge disorder is

$$\langle -\kappa|\hat{V}|\kappa\rangle = \frac{3}{2M(N+1)} \sum_m (\delta\varepsilon_m^A + e^{2i\theta(\kappa)} \delta\varepsilon_m^B), \tag{18}$$

which leads to the analytical estimate of the localization length

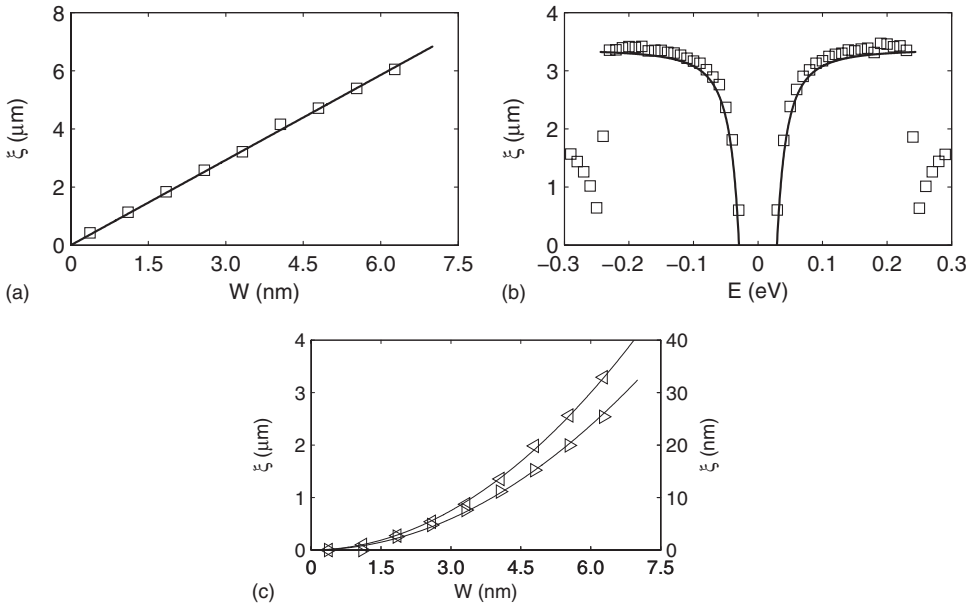

FIG. 2. Conductance localization length ξ of disordered graphene ribbons. Solid curves represent analytical estimates given by Eqs. (16), (19), and (22), and open symbols plots data from numerical transport calculations obtained using 10^4 random realizations over the disorder. (a) For short-range disorder throughout the ribbons, ξ is proportional to the width W of the ribbons for quasiparticles with energy $E=2E_g$. The disorder has been modeled through uncorrelated onsite energies with $\sigma_\varepsilon=0.087$ eV. (b) ξ as a function of energy for a 6.3-nm-wide ribbon with environmental edge disorder with $\sigma_\varepsilon=0.58$ eV. (c) The left (right) triangles together with the associated solid curve have been obtained assuming environmental (topological) edge disorder and should be read on the left (right) axis. In both cases, ξ scales with the square of the width ($E=2E_g$). The environmental and topological edge disorder use $\sigma_\varepsilon=0.58$ eV and $\sigma_w=0.16$ nm, respectively. For the latter disorder, $\lambda_t=0.10$.

$$\xi(E) \approx \lambda_e \frac{4W^2}{9d}\frac{\gamma^2}{\sigma_\varepsilon^2}\left(1-\frac{E_g^2}{4E^2}\right), \tag{19}$$

where λ_e is a factor that arises from a higher-order correction of the eigenvectors due to the edge interactions in Eq. (6); the wave function amplitude at the edge carbon sites is reduced 8%, leading to $\lambda_e \equiv (1-0.08)^{-4} \approx 1.4$. The energy dependence of the localization length can be seen in Fig. 2(b). Figure 2(c) shows the width dependence of the localization length for a case when $E \propto E_g$. This figure also shows an example of the localization length for a ribbon with topological edge disorder. The topological edge disorder has been modeled through edge roughness, where pairs of carbon atoms are added or removed with probability $p_0/(1+p_0)$. See Ref. 5 for more information on how such edges are generated and how steric problems are avoided. The edges have been assumed to be repassivated with hydrogen atoms after the edge disorder has been introduced. The addition and removal of atoms could be modeled through the introduction of new interaction paths between edge carbon sites of a ribbon without disorder. This approach leads to the potential

$$\hat{V} = \sum_{m=1}^{M} [\gamma \delta_{X_m^{(a)},1} c_{1,m-1}^{B\dagger} c_{1,m+1}^{A} - \gamma \delta_{X_m^{(r)},1} c_{N/2,m-1}^{B\dagger} c_{N/2,m+1}^{B}], \tag{20}$$

for the topological edge disorder, where δ is here the Kronecker delta and $X_{j'}^{(a)}$ and $X_{j'}^{(r)}$ are random variables that describe edges that allow for additions or removals of atoms, respectively. $P(X_{j'}^{(a)}=1)=p_0/(1+p_0)$ and $P(X_{j'}^{(a)}=0)=1/(1+p_0)$ are the probabilities of pairs of carbon atoms being added or not added at possible defect sites in the helical motif j'. $X_{j'}^{(r)}$ has the same probability distribution as $X_{j'}^{(a)}$. The backscattering matrix element of this potential is

$$\langle -\kappa|\hat{V}|\kappa\rangle = \frac{3\gamma}{2M(N+1)}\sum_m (\delta_{X_m^{(a)},1} - \delta_{X_m^{(r)},1}) \times \cos(2\kappa m + \theta). \tag{21}$$

Again using Eq. (13), the expression for the localization length can be obtained. For the topological disorder, herein, the expression is

$$\xi(E) \approx \lambda_t \frac{4W^2}{9d}\frac{3d^2}{\sigma_w^2}\left(1-\frac{E_g^2}{4E^2}\right), \tag{22}$$

where $\sigma_w^2/3d^2 = 2p_0/(1+p_0)^2$ is the variance of the ribbon width and λ_t is a factor that has been introduced to compensate for the fact that Eq. (20) does, in general, not describe weak disorder. When $p_0 \to 0$, however, the system is arguably weakly disordered and $\lambda_t \to 0.31$ converges. In this limit, λ_t is a parameter that compensates for higher-order corrections of the eigenvectors. Equation (22) is strictly only valid when $p_0 \ll 1$. Nevertheless, it seems to give approximate localization lengths for larger p_0 if λ_t is treated as a fitting parameter. Note that it is unlikely that Eq. (22) gives a quantitative prediction of the localization length for other examples of topological edge disorder; however, the main

characteristics are expected to be the same. In particular, the $\xi \propto W^2$ dependence of the localization length for $E \propto E_g$ should be valid for all first-order, uncorrelated edge disorder in armchair-edge graphene ribbons.

To verify the accuracy of the expressions for the localization lengths above, complete multiband transport calculations were preformed based on $G=(2e^2/h)\mathrm{Tr}(tt^\dagger)$,[27] where the trace was calculated using a Green function technique.[28] Numerical estimates of the localization length were then computed using $-(\partial\langle \ln G\rangle_{\mathrm{avg}}/\partial L)^{-1}$. Both the disordered ribbons and their leads, which have been assumed to be semi-infinite ribbons of the same type without disorder, were described by Hamiltonians that explicitly include both first- and third-nearest-neighbor interactions and edge interactions. The former Hamiltonian also included the disorder potentials that pertain to the considered type of disorder in the sample region. Note that the choice of leads should have no affect on the localization length. All numerical calculations showed that the analytical expressions for the localization length are reliable within the single-channel regime [cf. Fig. 2].

IV. DISCUSSION

The width dependences in Eqs. (16), (19), and (22) have several causes. First, it is important to realize that the total density of states is typically proportional to the number of atoms, and hence W. This W cancels out a usual W^{-1} factor from $|\langle -\kappa|\hat{V}|\kappa\rangle|^2$ in Eq. (13) for disorder through the material. Within the single-channel regime of armchair-edge ribbons, however, the total density of states is independent of the width, for $E \propto E_g$ [cf. Eq. (12)], and therefore, does not compensate the W^{-1} factor, leading to the scaling behavior seen in Fig. 2(a).[29] Second, edge disorder is, as the name suggests, confined to the edges, reducing the affected atoms and leading to $|\langle -\kappa|\hat{V}|\kappa\rangle|^2 \propto W^{-2}$. As the density of states is still width independent in the single-channel regime for $E \propto E_g$, the localization length in Fig. 2(c) must scale as $\xi \propto W^2$.

In both Figs. 2(a) and 2(c), the energy has been assumed to be proportional to the band gap. This assumption is not only made for convenience but also makes physical sense, as the band gap provides an energy scale near the Fermi level. Sometimes, however, it might not be desirable to relate the quasiparticle energy to the band gap; instead, the quasiparticle energy E could be assumed to be a fixed energy ΔE above the band edge $E_g/2$. Near the band edge, the dispersion of the two-band model can be expanded using effective mass theory, leading to $\varepsilon(k)=E_g/2+\hbar^2k^2/2m^*$, where $m^*=E_g/2v_F^2$. In this region, where the dispersion is parabolic, the parentheses in Eqs. (16), (19), and (22) can be expanded for small $\Delta E \ll E_g/2$, giving $(1-E_g^2/4E^2)\approx 2\Delta E/m^*v_F^2$. Typically, m^* is a constant, independent of the width of the material. In the armchair-edge graphene ribbons described herein, however, $m^* \propto W^{-1}$, thus introducing a width dependence to the localization length that in this parabolic region scales as $\xi \propto W^3$. As the quasiparticle energy is increased, the localization length scaling should exhibit a crossover from $\xi \propto W^3$ to $\xi \propto W^2$, the latter being the scaling in the region of linear dispersion, where $E_g^2/4E^2$ is small. The localization length in the region of linear dispersion is largely independent of the energy E and is also longer than in the region of parabolic dispersion [cf. Fig. 2(b)] for all widths. Because of the stronger width dependence of the localization length in the parabolic regime, one could imagine that the localization length would become longer than in the linear regime for a sufficiently large width. This is not the case, as evident from the factor $(1-E_g^2/4E^2)<1$ in Eqs. (16), (19), and (22), which shows that $\xi \to \xi_{\max}$ as $E_g^2/4E^2 \to 0$.

In electrical devices that exploit the difference in conductance between the "on" and "off" states, it is desirable that these states have sharp transitions between them. The sharpness of the transitions is expected to be related to the slope of the localization length near the band edge, which scales as $\partial\xi/\partial E=\xi_{\max}E_g^2/2E^3 \propto W^3$. That the slope is higher for wider ribbons has also been shown through numerical calculations.[5]

A key difference between environmental and topological edge disorder is how each scales with the hopping parameter γ. The environmental edge disorder potential is determined by external influence, herein modeled by an Anderson disorder potential that is independent of γ. However, a γ dependence enters the localization length in Eq. (13) through the group velocity and density of states. The expressions in Eqs. (11) and (12) lead to a localization length that scales as $\xi \propto \gamma^2$ [cf. Eq. (19)]. For topological edge disorder, on the other hand, the disorder potential, which describes additions or removals of paths, is proportional to γ in Eq. (20). As a consequence, the γ dependences from the velocity and density of states are cancelled out by the $|\langle -\kappa|\hat{V}|\kappa\rangle|^2 \propto \gamma^2$ factor in Eq. (13), leading to a localization length for topological edge disorder that is independent of γ [cf. Eq. (22)].

V. CONCLUSION

Because of the scaling of the localization length, one could conclude that wider strips are more robust against short-range edge disorder, especially if the disorder is confined to the strip edges. Owing to the scaling of the slope of the localization length, wider ribbons also have the advantage that they should exhibit a faster rise in the conductance near the band edges, as the quasiparticle energy is increased.

Another important point, highlighted by Fig. 2(c), is that the localization length in ribbons with topological edge disorder is typically much shorter than in ribbons with environmental edge disorder. This fact might in part explain why ballistic transport, so far, has been so elusive in experiments using narrow graphene ribbons, which have typically been plagued by topological edge disorder. It also emphasizes the importance of controlling the edges in graphene ribbons, in particular, the narrow ones. Hopefully, techniques such as nanocutting,[30–32] Joule heating,[33] and unzipping of carbon nanotubes[34,35] could lead to great improvements in this area.

ACKNOWLEDGMENTS

This work is supported by the Office of Naval Research, directly and through the Naval Research Laboratory.

[1] C. Berger *et al.*, Science **312**, 1191 (2006).
[2] M. Y. Han, B. Özyilmaz, Y. Zhang, and P. Kim, Phys. Rev. Lett. **98**, 206805 (2007).
[3] P. L. McEuen, M. S. Fuhrer, and H. Park, IEEE Trans. Nanotechnol. **1**, 78 (2002).
[4] D. A. Areshkin, D. Gunlycke, and C. T. White, Nano Lett. **7**, 204 (2007).
[5] D. Gunlycke, D. A. Areshkin, and C. T. White, Appl. Phys. Lett. **90**, 142104 (2007).
[6] Y. Yoon and J. Guo, Appl. Phys. Lett. **91**, 073103 (2007).
[7] D. Querlioz, Y. Apertet, A. Valentin, K. Huet, A. Bournel, S. Galdin-Retailleau, and P. Dollfus, Appl. Phys. Lett. **92**, 042108 (2008).
[8] M. Wimmer, I. Adagideli, S. Berber, D. Tománek, and K. Richter, Phys. Rev. Lett. **100**, 177207 (2008).
[9] N. Nemec, K. Richter, and G. Cuniberti, New J. Phys. **10**, 065014 (2008).
[10] A. Cresti, N. Nemec, B. Biel, G. Niebler, F. Triozon, G. Cuniberti, and S. Roche, Nano Res. **1**, 361 (2008).
[11] M. Evaldsson, I. V. Zozoulenko, H. Xu, and T. Heinzel, Phys. Rev. B **78**, 161407(R) (2008).
[12] E. R. Mucciolo, A. H. Castro Neto, and C. H. Lewenkopf, Phys. Rev. B **79**, 075407 (2009).
[13] A. Cresti and S. Roche, Phys. Rev. B **79**, 233404 (2009).
[14] F. Tseng, D. Unluer, K. Holcomb, M. R. Stan, and A. W. Ghosh, Appl. Phys. Lett. **94**, 223112 (2009).
[15] G. Schubert, J. Schleede, and H. Fehske, Phys. Rev. B **79**, 235116 (2009).
[16] Y.-W. Son, M. L. Cohen, and S. G. Louie, Phys. Rev. Lett. **97**, 216803 (2006).
[17] D. Gunlycke and C. T. White, Phys. Rev. B **77**, 115116 (2008).
[18] P. W. Anderson, Phys. Rev. **109**, 1492 (1958).
[19] N. M. Makarov and Y. V. Tarasov, Phys. Rev. B **64**, 235306 (2001).
[20] C. T. White, J. Li, D. Gunlycke, and J. W. Mintmire, Nano Lett. **7**, 825 (2007).
[21] P. R. Wallace, Phys. Rev. **71**, 622 (1947).
[22] K. Nakada, M. Fujita, G. Dresselhaus, and M. S. Dresselhaus, Phys. Rev. B **54**, 17954 (1996).
[23] L. Brey and H. A. Fertig, Phys. Rev. B **76**, 205435 (2007).
[24] D. Gunlycke and C. T. White, Appl. Phys. Lett. **93**, 122106 (2008).
[25] V. Barone, O. Hod, and G. E. Scuseria, Nano Lett. **6**, 2748 (2006).
[26] D. J. Thouless, J. Phys. C **6**, L49 (1973).
[27] D. S. Fisher and P. A. Lee, Phys. Rev. B **23**, 6851 (1981).
[28] T. N. Todorov, G. A. D. Briggs, and A. P. Sutton, J. Phys. Condens. Matter **5**, 2389 (1993).
[29] C. T. White and T. N. Todorov, Nature (London) **393**, 240 (1998).
[30] S. S. Datta, D. R. Strachan, S. M. Khamis, and A. T. C. Johnson, Nano Lett. **8**, 1912 (2008).
[31] L. Ci, Z. Xu, L. Wang, W. Gao, F. Ding, K. F. Kelly, B. I. Yakobson, and P. M. Ajayan, Nano Res. **1**, 116 (2008).
[32] L. C. Campos, V. R. Manfrinato, J. D. Sanchez-Yamagishi, J. Kong, and P. Jarillo-Herrero, Nano Lett. **9**, 2600 (2009).
[33] X. Jia *et al.*, Science **323**, 1701 (2009).
[34] D. V. Kosynkin, A. L. Higginbotham, A. Sinitskii, J. R. Lomeda, A. Dimiev, B. K. Price, and J. M. Tour, Nature (London) **458**, 872 (2009).
[35] L. Jiao, L. Zhang, X. Wang, G. Diankov, and H. Dai, Nature (London) **458**, 877 (2009).